Vol. 498: 55–71, 2014
doi: 10.3354/meps10616

MARINE ECOLOGY PROGRESS SERIES
Mar Ecol Prog Ser

Published February 17

Factors controlling phytoplankton physiological state around the South Shetland Islands (Antarctica)

Cristina García-Muñoz[1,*], Cristina Sobrino[2], Luis M. Lubián[1], Carlos M. García[3], Sandra Martínez-García[2,5], Pablo Sangrà[4]

[1]Departamento de Ecología y Gestión costera, Instituto de Ciencias Marinas de Andalucía (ICMAN-CSIC), 11510 Puerto Real, Cádiz, Spain

[2]Departamento de Ecoloxía e Bioloxía Animal, Universidade de Vigo, 36200 Vigo, Pontevedra, Spain

[3]Departamento de Biología, Facultad de Ciencias del Mar y Ambientales, Universidad de Cádiz, 11510 Puerto Real, Cádiz, Spain

[4]Departamento de Física, Facultad de Ciencias del Mar, Universidad de Las Palmas de Gran Canaria, Campus de Tafira, 35017 Las Palmas de Gran Canaria, Spain

[5]*Present address:* C-MORE, University of Hawaii, C-MORE Hale, 1950 East West Road, Honolulu, Hawaii 96822, USA

ABSTRACT: To investigate factors controlling phytoplankton physiological state around the South Shetland Islands, phytoplankton abundance and structure, fluorescence properties, photoprotective pigment composition and physicochemical variables were studied. Nanophytoplanktonic cells (<20 µm) contributed 84% of total chlorophyll *a* (chl *a*), except for the station closest to the Antarctic Peninsula where microplanktonic cells (>20 µm) predominated (up to 85% of total chl *a*). Daily irradiance over the mixed layer depth (MLD) was inversely related with integrated nanoplanktonic chl *a*; however, its relative contribution to total chl *a* increased at mid-irradiance values. The average maximum quantum yield of photosystem II (F_v/F_m) below 20 m depth ranged from 0.17 to 0.53 and showed that cells were under suboptimal physiological conditions in the Drake region, but had higher performance around the South Shetland Islands and towards the Antarctic Peninsula. A reverse pattern in the fluorescence yield was detected. A deeper examination of the F_v/F_m vertical profiles according to the sampling time detected surface photoinhibition during the day and a spatial modulation of F_v/F_m related to irradiance and the silicic acid:nitrate ratio. It appears that cells' photosynthetic performance was controlled by iron limitation in the Drake region, whereas irradiance regime controlled phytoplankton physiological state in the rest of the studied regions. Vertical mixing differences among stations, the relative position of the euphotic layer depth with respect to the MLD and the photoprotective pigment ratios revealed contrasting responses to light stress among the different phytoplanktonic groups, revealing a better adaptation of medium size cells, especially diatoms, to stratified waters receiving high irradiance.

KEY WORDS: South Shetland Islands · Phytoplankton · F_v/F_m · Irradiance · Size · Mixed layer · Nutrients

INTRODUCTION

The phytoplankton composition in coastal and frontal regions of Antarctic waters has been extensively described over the past several decades. The oldest studies tended to emphasize the abundance of microplanktonic diatoms (Hart 1942), probably due to the lack of techniques that allowed the detection and analysis of smaller cells. Later, especially after the autofluorescent properties of photosynthetic plankton started to be exploited by flow cytometry (FCM), it was realized that pigmented flagellates (prymnesiophytes, cryptophytes, prasinophytes) and other groups (diatoms) in the size range of nano-

*Corresponding author: cristina.garcia@icman.csic.es

plankton (2 to 20 µm equivalent spherical diameter [ESD]) were the main components of the planktonic community in the Southern Ocean (e.g. Hewes et al. 1990, 2009, Rodríguez et al. 2002). Especially in the Bransfield Strait, nanoflagellates account for 80% of the total phytoplankton carbon (Kang & Lee 1995, Kang et al. 2001). Independent of cell size, in oceanic Antarctic waters, factors such as the mixed layer depth (MLD), the advection caused by strong winds and storms, the presence of limiting micronutrients, such as iron, and the daily irradiance variations have been invoked to explain low phytoplankton biomass (e.g. Priddle et al. 1994, Varela et al. 2002, Alderkamp et al. 2010, Vernet et al. 2012). Limitation of summer phytoplankton accumulation due to low iron availability and deep mixed layers has been observed in the Drake Passage (Hewes et al. 2009, Alderkamp et al. 2011). In contrast, the Bransfield Strait and the waters surrounding the South Shetland Islands (SSI) have a relatively high iron concentration due to the proximity of the Weddell Sea (Hewes et al. 2008, Ardelan et al. 2010) and the continent itself (De Jong et al. 2012). Recent iron enrichment experiments (SOFeX: Coale et al. 2004; LOHAFEX: Mazzochi et al. 2009) clearly demonstrate iron's role in controlling phytoplankton processes in surface Antarctic waters, though the response to iron additions strongly varies depending on background silicic acid concentrations (Sarmiento et al. 2004). Fast repetition rate fluorometry (FRRF) has been used as a survey tool to assess the physiological status of phytoplankton assemblages under close to real-time conditions (Kolber & Falkowski 1993). Direct relationships between the maximum photosynthetic efficiency (F_v/F_m) and iron concentrations have been already reported (e.g. Gervais et al. 2002, Sosik & Olson 2002, Hopkinson et al. 2007). Behrenfeld et al. (2006) classified the physiological regime of polar waters as type IV, with low dawn F_v/F_m values and small nocturnal decreases in F_v/F_m due to iron limitation, nitrate repletion and low phytoplankton growth rates. Exposure to photosynthetically active radiation (PAR) and ultraviolet radiation (UVR) can also be responsible for a decrease in F_v/F_m (Van de Poll et al. 2011, Neale et al. 2012), especially in the Southern Ocean where vertical mixing and the effects of excess near-surface irradiance are particularly important (e.g. Vaillancourt et al. 2003, Alderkamp et al. 2010, 2011, Neale et al. 2012).

In this context, different laboratory studies have investigated variations in the fluorescence-derived photosynthetic properties of phytoplankton groups under different light (Kropuenske et al. 2009, 2010, Mills et al. 2010) and nutrient conditions (Geider et al. 1993), or the synergy of both (Van de Poll et al. 2005). Kropuenske et al. (2009, 2010) and Mills et al. (2010) investigated the response of 2 main Antarctic phytoplankton groups (haptophytes and diatoms) exposed to different irradiance regimes using phytoplankton cultures under controlled conditions, and concluded that diatoms might be more successful in stable irradiance regimes, such as the constant low-irradiance environment of sea ice or the high-irradiance regime of a stratified, shallowly mixed water column. The physiological response of phytoplankton to several *in situ* physicochemical conditions in the Southern Ocean, with a special emphasis on iron and light limitation, has also received growing attention (Vaillancourt et al. 2003 in the East Antarctica, Alderkamp et al. 2010 in the Drake Passage, Feng et al. 2010 in the Ross Sea, Arrigo & Alderkamp 2012, and references therein, in the Amundsen Sea). But the Antarctic Peninsula tip and particularly the SSI area remain poorly studied in this sense.

García-Muñoz et al. (2013a) previously analyzed the phytoplankton assemblages with regard to water masses and mesoscale physical structures (fronts and eddies) around the SSI, and concluded that the distribution and composition of the different phytoplanktonic groups were strongly affected by the position of the fronts and the physical gradients (temperature and salinity). The goal of this second study was to investigate which physicochemical variables (light regime and nutrients) were affecting the phytoplankton physiological state through the study of the photoprotective pigment ratios and vertical measurements of the photosynthetic efficiency in the surroundings of the SSI (Drake Passage, the SSI shelf, the Bransfield Strait and the Antarctic Sound). Furthermore, we compared the physiological responses of phytoplankton among stations with different mixing conditions, with regard to the predominance of nanoplanktonic vs. microplanktonic phytoplankton cells. For this purpose, the mesoscale area studied is an excellent system to investigate patterns in Antarctic phytoplankton physiology, as it includes a wide range of biological and physicochemical conditions.

MATERIALS AND METHODS

Field sampling and oceanographic measurements

The COUPLING expedition (8 to 27 January 2010) was conducted onboard RV 'Hespérides' around the SSI, with a main transect sampled from Drake Pas-

sage to Bransfield Strait (Fig. 1). Hydrographic data were collected using a Seabird 911plus CTD probe with a Seapoint fluorescence sensor, to detect the deep fluorescence maximum (DFM), coupled to an oceanographic rosette. The MLD was inferred from temperature and salinity profiles using the algorithm of Kara et al. (2000). Simultaneous shipboard wind speeds were obtained from a continuously recording Young 05103 sensor and recorded as 1 min mean. PAR (λ = 400 to 700 nm) throughout the water column (I_z, µmol photons m^{-2} s^{-1}) was measured with a Satlantic OCP-100FF radiometer attached to the rosette. The incident downwelling irradiance was continuously monitored on deck with a Kipp & Zonen CM11 sensor. Daily PAR at the surface was estimated as the sum of the average surface solar irradiance each hour (W m^{-2}) and a factor of 2.08 mol photons m^{-2} s^{-1} MW^{-1} (Ting & Giacomelli 1987). To obtain the total daily PAR in the upper mixed layer (I_{MLD}, mol photons m^{-2} d^{-1}), the average daily irradiance just below the sea surface (I_o) was estimated using 0.8 as the transmittance at the air–sea interface (Figueiras et al. 1999) and was calculated as:

$$I_{MLD} = \Sigma[I_o \times \exp(-K_d \times z)]/MLD \quad (1)$$

where K_d is the PAR attenuation coefficient (m^{-1}) and z is depth (m).

Size fractionated chlorophyll *a*

Chlorophyll *a* (chl *a*) concentration was determined fluorometrically. Water samples (250 ml) were sequentially filtered through 20, 2 and 0.2 µm polycarbonate membrane filters and pigments were extracted overnight in 90% acetone at –20°C. Fluorescence was measured on a Turner TD-700 fluorometer that had been calibrated with pure chl *a* following the UNESCO (1994) standard protocol. Fluorescence yield, as a qualitative index for physiological stress (Maxwell & Johnson 2000, Beardall et al. 2001), was calculated as the ratio of the CTD profiling fluorometer reading (log mV) to the chl *a* concentration (log [µg m^{-3}]) measured for each bottle, as desribed in Hewes et al. (2009).

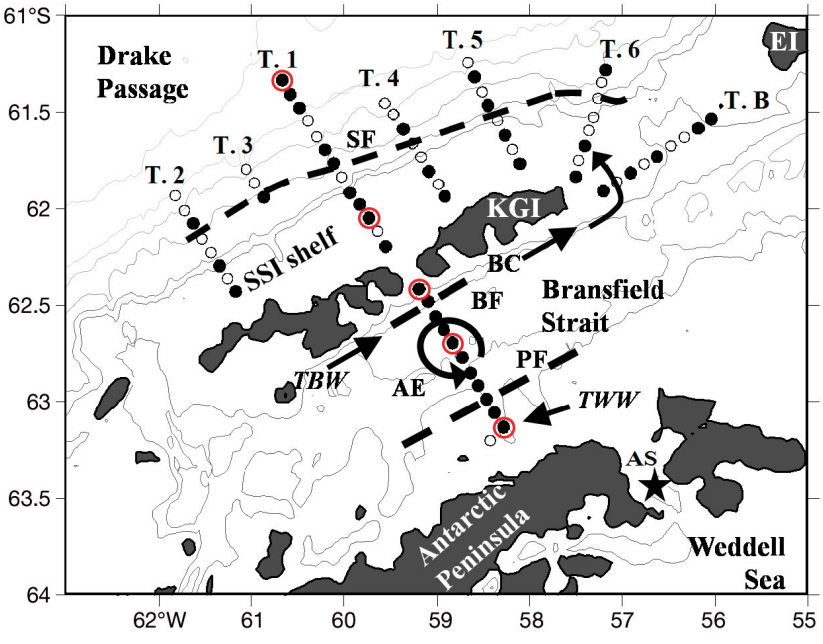

Fig. 1. Area of study and location of stations and transects (T.1 to T.6, T.B). Black dots represent those stations sampled with fast repetition rate fluorometry (FRRF). To follow circadian cycles of Antarctic phytoplankton, the station at the Antarctic Sound (AS) was sampled 3 times a day, including 4 FRRF casts. AE: anticyclonic eddy; BF/BC: Bransfield Front/Bransfield Current; EI: Elephant Island; KGI: King George Island; PF: Peninsula Front; SF: Shetland Front; TBW: Transitional Bellingshausen Water; TWW: Transitional Weddell Water. Grey lines represent bathymetry (500, 1000, 2000, 3000, 4000 and 5000 m). Stations with a red circle were used to represent vertical profiles in Figs. 2, 3 & 6

Macronutrient determination

Water samples for macronutrient analysis (nitrate, nitrite, ammonium, phosphate and silicic acid) were poured directly from the Niskin sampling bottle on the carousel into clean polyethylene vials (5 ml). Samples were collected from the surface to 1000 m depth (when bathymetry allowed) at fixed depths (5, 10, 25, 50, 75, 100, 150, 200, 300, 500 and 1000 m, including the DFM). Samples were filtered through 0.45 µm (Minisart NY 25) and stored frozen (–80°C) until analysis using a Technicon TRAACS 800 and Skalar San ++ System Autoanalyzers following standard protocols (Grasshoff et al. 1983).

Flow cytometry analysis

A volume of 20 ml was used for FCM observation of cell populations. Fresh samples from 6 depths (5, 10, 25, 50, 75 and 100 m, including the DFM) were collected and fixed with a mix of 1% paraformaldehyde and 0.05% glutar-

aldehyde. Samples were analysed onboard with a FACScalibur flow cytometer (Becton Dickinson). Phytoplankton counts were obtained at a high flow rate (1.05 µl s^{-1}) over 10 min. Flow rate was calibrated at the beginning and end of the sampling period (Rodríguez et al. 2002). Data were acquired with the CellQuest software as List Mode Standard files and later analysed with CellQuest (Becton Dickinson) and WinMDI 2.9 (Joseph Trotter 1993–2000). Three size groups of eukaryotic cells were discriminated on the bivariate plots of side light scatter versus red fluorescence (FL3): 'nano small' (2.8 ± 0.2 µm ESD), 'nano medium' (5.2 ± 0.4 µm ESD) and 'nano large' (8.7 ± 0.6 µm ESD). A fourth characteristic population within the nanoplankton size category is 'cryptophytes' (11.3 ± 1.4 µm ESD), easily separated from the other groups by the orange fluorescence of phycoerythrin (FL2). The transformation of the side light scatter signal to cell volume was carried out through a calibration curve before the cruise. Further details are already published elsewhere (García-Muñoz et al. 2013a).

Pigment analysis

Seawater samples (2 to 5 l) were collected from the surface and the DFM. They were filtered onto 47 mm Whatman glass fiber filters (GF/F, 0.7 µm nominal pore size) and kept frozen (–80°C) until pigment analyses were carried out on a high-performance liquid chromatography (HPLC) system. Pigment extraction, separation and sample processing were performed according to Zapata et al. (2000). The array of phytoplankton pigments found in this study includes photosynthetic and photoprotective carotenoids. The ratio of the sum of photoprotective carotenoids (PPC; alloxanthin [Allox], diadinoxanthin [Dd] and diatoxanthin [Dt] in our study) to the sum of total pigments (TP) was used as an indicator of the phytoplankton physiological adaptation to the prevailing ambient light (Mendes et al. 2012). In diatoms and haptophytes, non-photochemical quenching is specifically related to the presence of Dt rather than Dd (Olaizola et al. 1994, Alderkamp et al. 2010). However, because xanthophyll cycle pigments are epoxidated on a timescale of minutes (Van de Poll et al. 2006, Alderkamp et al. 2010), faster than the time required to process and filter samples by the method used in this study, all the Dt was converted to Dd and only trace amounts of Dt were detected in some samples. Additional information about the pigment extraction protocol is published elsewhere (García-Muñoz et al. 2013a).

Variable fluorescence measurements

The photo-physiological state of natural phytoplankton was measured with a FRRF (Chelsea Instruments) for all casts. Vertical profiles were assessed at 44 different locations of the study area. A particular station located at the Antarctic Sound was sampled 4 times (CD1 to CD4) to follow phytoplankton responses during a circadian cycle (Fig. 1). The profiling protocol was structured to optimize data quality in the upper few meters, as described in Neale et al. (2012). For all casts, data were combined from 2 or 3 sequential vertical ascents. Two profiles were taken starting from below the mixed layer followed by two from 30 m, at 10 m min^{-1}. The slow ascent rate and extra profiling in the upper 30 m was to ensure adequate coverage in the photoactive zone, which is characterized by strong vertical gradients in irradiance and fluorescence. The instrument was mounted on the winch cable in a vertical position with the optical ports on the top, allowing data acquisition to continue up to the surface. Saturating-chain sequences of 100 1.1 µs flashes were applied at 2.8 µs intervals. Fluorescence transients were logged internally during profiling from the average of 16 successive sequences. Data were alternately acquired from the open ('light') and enclosed ('dark') chambers every 100 ms. All data were processed using FRS software (Chelsea Technologies), correcting for instrument response function and a seawater blank. The latter was obtained by filtering water from each station using 0.2 µm pore filters. Values shown in the paper correspond to those acquired with the dark chamber to calculate dark-adapted maximum quantum efficiency, $F_v/F_m = (F_m - F_0)/F_m$, where F_0 and F_m are the minimum and maximum fluorescence rate after saturating-chain sequences, respectively, when all the reaction centers are closed. This notation was chosen for practical purposes since, despite the slow profiling speed, only measurements below the euphotic zone or determined at night could be regarded as completely dark-adapted maximal quantum efficiency. Vertical distribution of PAR (400 to 700 nm) was also measured using a hemispherical quantum sensor (CI PAR, Chelsea Instruments), which was provided as standard with the FRRF. The euphotic layer depth (z_{eu}) was defined as the depth at which the light intensity was attenuated to 1% of the value just below the surface, and was calculated as $z_{eu} = \ln(0.01)/K_d$. Values of K_d were calculated over the depth that PAR measurements were reliable, as shown in Vaillancourt et al. (2003).

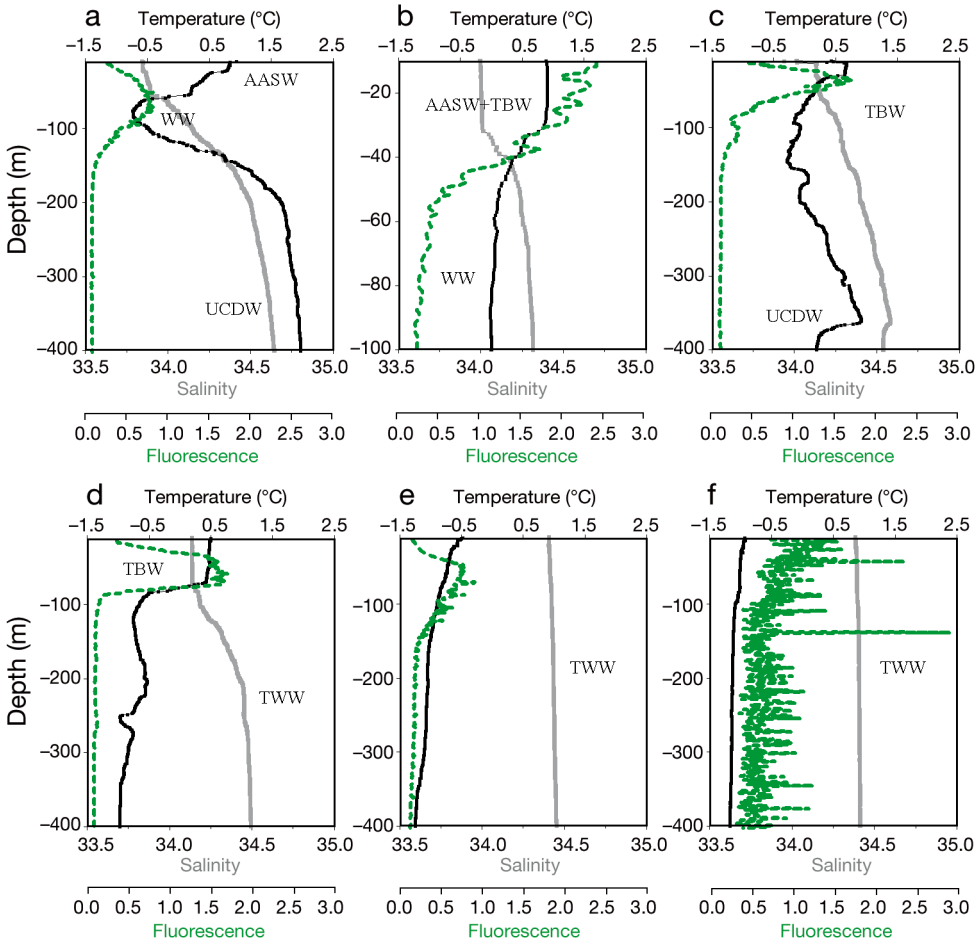

Fig. 2. Vertical profiles of temperature (°C; black line), salinity (grey line) and fluorescence (green dashed line) across the different regions: (a) the Drake region; (b) the northern shelf of the South Shetland Islands (SSI); (c) between the southern SSI shelf and the Bransfield Front; (d) in the middle of the Bransfield Strait; (e) south of the Peninsula Front; (f) Antarctic Sound (CD1 cast). UCDW: Upper Circumpolar Deep Water; TWW: Transitional Weddell Water; AASW: Antarctic Surface Water; WW: Winter Water; TBW: Transitional Bellingshausen Water, TWW: Transitional Weddell Water

To study the relative contribution of physicochemical factors (salinity, temperature, vertical PAR [values from the FRRF PAR sensor] and macronutrients) that could account for most of the variability observed in the F_v/F_m values, a multiple linear regression analysis was used. To obtain the best-fitting model, we used the 'stepwise forward' method. The model with the lowest Akaike's information criterion (AIC) was chosen as the most parsimonious. Deviance changes, the degree of difference between the observed frequencies and those predicted by the models, were also examined as a measure of the goodness of fit.

RESULTS

Physicochemical and biological environment

As shown in Fig. 1 and detailed in previous studies around the SSI (e.g. García et al. 2002, Sangrà et al. 2011, García-Muñoz et al. 2013a), this region has high mesoscale variability due to the confluence of different water masses and the presence of mesoscale physical features such as fronts and eddies. Therefore, according to the locations of mesoscale structures (Fig. 1) and water mass distribution we distinguished 6 different regions: the Drake Passage region north of the Shetland Front (SF), the northern shelf of the SSI region located south of the SF, the Bransfield frontal region between SSI and the Bransfield Front (BF), the middle Bransfield region located between the BF and the Peninsula Front (PF) where an anticyclonic eddy (AE) was detected, the region south of the PF and the Antarctic Sound (AS) point. Fig. 2 shows vertical profiles of temperature, salinity and fluorescence for each of these regions. In the Drake Passage (Fig. 2a), the warm (>0.5°C) Antarctic Surface Water (AASW) occupied the upper layers, with Winter Water (WW) immediately below, identified by minimum subsurface temperature values and higher salinity. Deep DFMs (between 60 and 90 m) were detected in this region (Fig. 2a). Below 200 m depth, the relatively warm (*in situ* and potential temperature >0°C) and salty (>34.5) Upper Cir-

cumpolar Deep Water (UCDW) was detected. In the northern shelf of SSI south of the SF, UCDW disappeared and WW spread throughout the water column reaching the bottom. The upper layer was characterized by a mixture of AASW and the warmer and well-stratified Transitional Zonal Water with Bellingshausen Sea influence (TBW) due to the intrusion of the Bransfield Current (BC) when recirculating around the SSI. Shallow DFMs (from surface to 25 m) were also detected (Fig. 2b). In the BF region, a narrow tongue of UCDW reappeared (Fig. 2c) around 300 m, as previously described by Sangrà et al. (2011). In the middle Bransfield region, TBW spread from the BC at the surface, laying over the cooler and denser Transitional Zonal Water with Weddell Sea influence (TWW), which occupies the main body of the strait (Fig. 2d). The DFM followed the same trend as the MLD (see Fig. 2 in García-Muñoz et al. 2013a), deepening in the middle of the strait. Although the region south of the PF and the AS were both influenced by TWW (Fig. 2e,f), we decided to separate them due to the different fluorescence profiles detected and the large distance between sampling points. Notice that temperature and salinity are almost constant over the water column, indicating that TWW is a rather homogeneous water mass without noticeable stratification and very deep mixed layers that used to reach the bottom. Deep DFMs (between 50 and 75 m) were detected south of the PF, but fluorescence profiles at AS were discontinuous showing numerous spikes (Fig. 2e,f).

During the cruise, summer daylength was 16 h on average. Levels of incident surface PAR and total daily PAR were highest at stations sampled within the first part of the cruise (8 to 11 January) in the central Bransfield Strait (49.1 mol photons m^{-2} d^{-1}, mean daily PAR), while they decreased north of 62°S latitude and in the Antarctic Sound, due to a slightly decreasing daylength and increasing cloudiness (27.3 mol photons m^{-2} d^{-1}, mean daily PAR). To study the physiological response of phytoplankton to different irradiances, we considered day stations to be those sampled between dawn (06:00 to 10:00 h) and 18:00 h, and night stations to be those sampled between dusk (18:00 to 22:00 h) and 06:00 h (local time). Underwater surface irradiance at stations sampled during daylight ranged from 33 µmol photons m^{-2} s^{-1} (early in the morning on a very cloudy day) to 800 µmol photons m^{-2} s^{-1}, while irradiance at stations sampled at dawn ranged from 0 µmol photons m^{-2} s^{-1} to 38 µmol photons m^{-2} s^{-1}. Within regions, average levels of total daily PAR in the upper mixed layer (I_{MLD}) were highest in the Drake region (on average 8.55 mol photons m^{-2} d^{-1}). The lowest values (<3.5 mol photons m^{-2} d^{-1}) coincided with those regions where deep MLDs were detected, especially in the AS (Fig. 3), where the MLD reached 250 m depth. In contrast, at the BF and PF stations, I_{MLD} reached the highest values (17.5 and 14.0 mol photons m^{-2} d^{-1}, respectively) due to the shallowing of the MLD. North of the SF, the z_{eu} was found at ~100 m, becoming shallower towards the SSI shelf (50 to 60 m) and exceeding the MLD at all stations. Compared with these regions, we found deeper MLDs (>75 m) than the z_{eu} in the Bransfield Strait at 3 specific sites: between the archipelago and the BF, in the middle of the strait and in those stations south of the PF. Conversely, at the stations where the mesoscale fronts (BF and PF) were located, the z_{eu} was deeper than the MLD.

The average concentrations of silicic acid, nitrate and phosphate in the mixed layer were high (>65, >25 and >1.8 µM, respectively) throughout the entire study region south of the SF, increasing towards the AS. In contrast, silicic acid concentrations decreased to values close to 40 µM in the Drake region (Table 1), whereas nitrate and phosphate remained constant. Si* tracer (calculated as the concentration of silicic acid minus nitrate), defined by Sarmiento et al. (2004) as a proxy for iron limitation in the sampling area, followed the same trend, with significantly lower values (Tukey's post hoc honestly significant difference test, $p < 0.05$) in the Drake region compared with the other regions (Table 1). Vertical Si* profiles revealed negative values in surface waters of the Drake region (Fig. 3a) related to AASW. Rather uniform profiles were detected at the Bransfield Strait and in the AS (Fig. 3d,f), whereas at both edges of the Bransfield Strait, Si* showed sawtooth profiles ranging from 10 to over 50 (Fig. 3c,e). Average ammonium concentrations were higher north of the archipelago than in the southern regions. The N/P ratio was constant in almost all regions with values close to the Redfield ratio (15 to 16), except in the region between SSI and BF where low ratios were detected (<14) and the AS, where the ratios increased to 18.

Vertical profiles of chl *a* revealed contrasting concentrations between stations located in the Drake region (<0.5 mg m^{-3}) and the rest of the regions. The highest chl *a* values were recorded in the AS (up to 2.5 mg m^{-3}) followed by the northern SSI shelf and the Bransfield region (Fig. 3). On average, the contribution of phytoplanktonic cells <20 µm ESD was 84% of total chl *a*, except for the AS, where microplanktonic size range (>20 µm ESD) predomi-

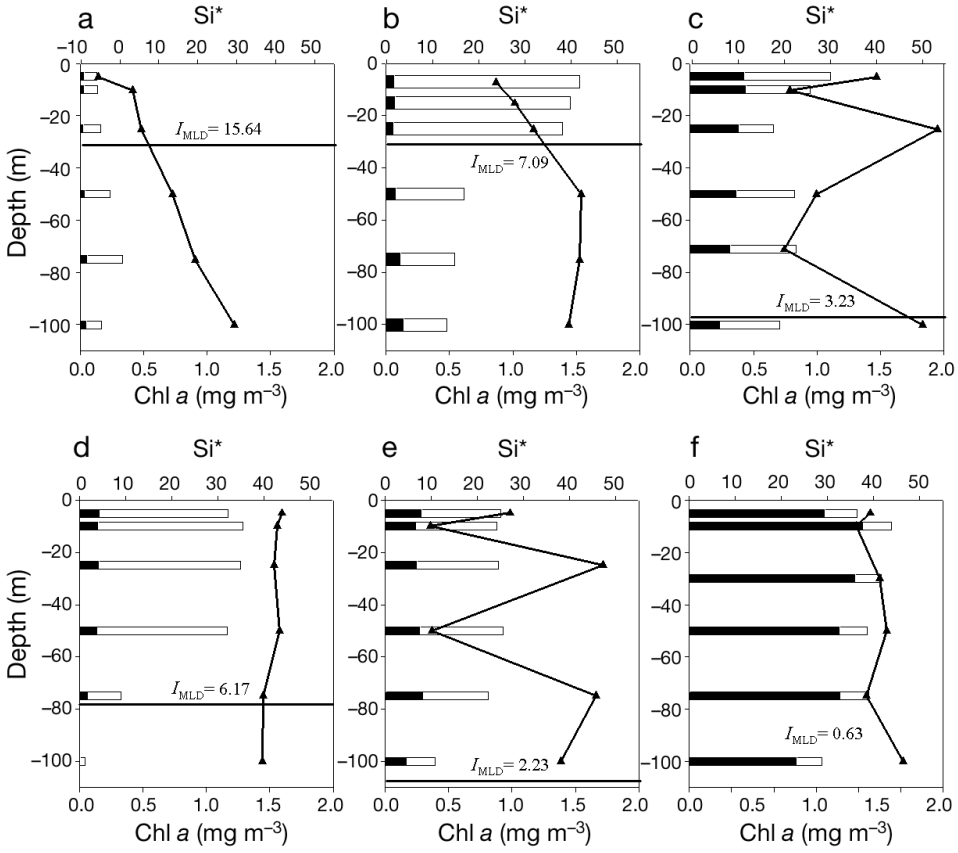

Fig. 3. Vertical profiles of fractionated chlorophyll *a* concentrations (mg m^{-3}) (white bars: chl *a* < 20 µm equivalent spherical diameter [ESD], black bars: chl *a* > 20 µm ESD) and Si* (concentration of silicic acid minus nitrate) across the different regions: (a) the Drake region; (b) the northern shelf of the South Shetland Islands (SSI); (c) between the southern SSI shelf and the Bransfield Front; (d) in the middle of the Bransfield Strait; (e) south of the Peninsula Front; (f) Antarctic Sound (CD1 cast). Solid horizontal line represents the MLD. Total daily photosynthetically active radiation in the upper mixed layer (I_{MLD}, mol photons m^{-2} d^{-1}) at each station is indicated. Note the different scale for chl *a* in (f) and the negative Si* values in the upper layer of (a)

nated (up to 85% of total chl *a*). Both chl *a* fractions concentrations were significantly positively correlated with the Si* ratio ($p < 0.01$, N = 253). However, different patterns were detected in the size-fractionated chl *a* concentration between regions with different mixing depths, with increasing chl *a* > 20 µm ESD values as the MLD deepened (Fig. 3c,e,f). To further explore this relationship, fractionated chl *a* was depth integrated (mg m^{-2}) from the surface to the MLD at each station and compared with I_{MLD} (mol photons m^{-2} d^{-1}). Although chl *a* < 20 µm ESD decreased exponentially as the I_{MLD} increased (Fig. 4), its relative

Table 1. Mean (±SD) within the mixed layer depth of all macronutrient concentrations (µM) and ratios between N (nitrate + nitrite) and phosphate (P) and silicic acid minus nitrate (Si*) across the different hydrographic regions

	Nitrate (µM)	Nitrite (µM)	Ammonium (µM)	Silicic acid (µM)	Phosphate (µM)	Si*	N/P
Drake region	27.67 (3.35)	0.71 (0.30)	0.67 (0.16)	37.20 (6.37)	1.83 (0.12)	9.53 (6.94)	15.59 (2.10)
Northern shelf	29.56 (3.42)	0.58 (0.28)	0.47 (0.25)	69.56 (8.53)	1.79 (0.10)	40.00 (8.27)	16.89 (2.27)
South Shetland Islands–Bransfield Front	25.51 (1.37)	0.16 (0.02)	0.38 (0.12)	65.66 (5.72)	1.91 (0.09)	40.15 (7.09)	13.46 (0.04)
Bransfield Strait	29.55 (3.07)	0.56 (0.28)	0.50 (0.24)	70.10 (7.88)	1.82 (0.12)	40.54 (7.85)	16.67 (2.20)
South of Peninsula Front	31.88 (3.94)	0.54 (0.28)	0.44 (0.18)	70.38 (11.49)	2.02 (0.06)	38.50 (12.82)	15.96 (2.00)
Antarctic Sound	34.97 (3.32)	0.68 (0.10)	0.32 (0.15)	73.56 (6.29)	2.01 (0.05)	38.58 (8.43)	17.78 (1.69)

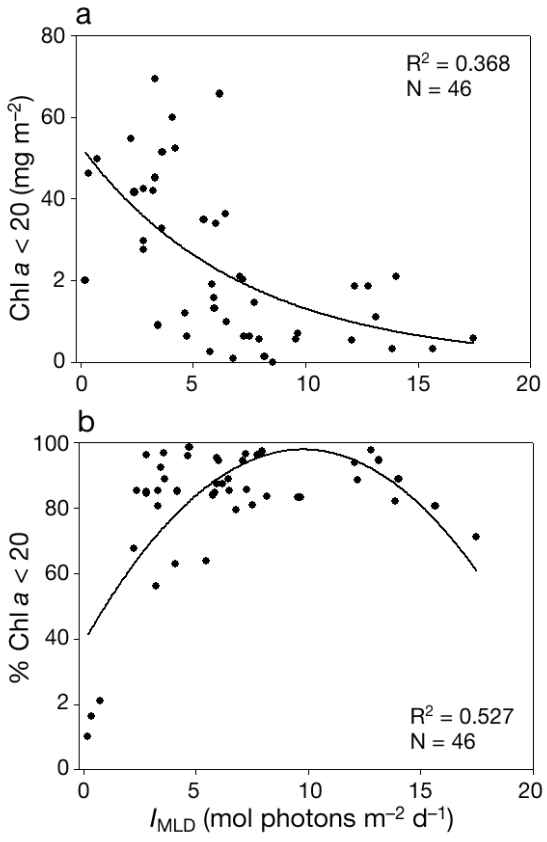

Fig. 4. (a) Exponential relationship between total daily photosynthetically active radiation in the upper mixed layer (I_{MLD}, mol photons m^{-2} d^{-1}) and chl *a* <20 µm equivalent spherical diameter (ESD) concentrations (mg m^{-2}) ($y = 52.74e^{-0.14x}$) and (b) 2nd order polynomial regression between I_{MLD} and the relative contribution of chl *a* <20 µm ESD (%) to total chl *a* ($y = -0.62x^2 + 12.09x + 38.90$)

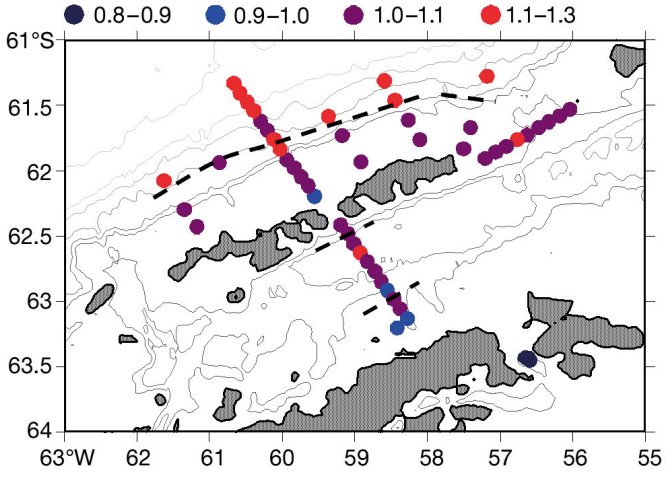

Fig. 5. Mean mixed layer depth fluorescence yield (log mV/log µg chl *a*), used as a proxy for iron-stressed photosynthesis throughout the study area. Dashed lines represent the locations of the fronts, as in Fig. 1

contribution (%) to total chl *a* increased following a 2nd order polynomial regression until a maximum was detected at mid-irradiances (I_{MLD} = 9.74 mol photons m^{-2} d^{-1}) (Fig. 4). The average fluorescence yield (Fig. 5) in the MLD was lower in the AS, becoming higher towards the Drake region, following a reverse pattern of total chl *a*. A significant negative correlation was detected between this physiological index and the I_{MLD} ($r = 0.38$, $p < 0.05$, $N = 51$).

Nanophytoplankton composition was on average numerically dominated by 'nano medium' cells (76.3%) followed by 'nano small' (20.1%), 'nano large' (3.1%) and cryptophytes (0.5%). Overall, the highest nanophytoplanktonic abundances (>6000 cells ml^{-1}) were reached around the SSI shelf and in the middle of the Bransfield Strait (Fig. 6b,d), whereas the lowest abundances (<2000 cells ml^{-1}) were detected between the SSI and the BF and in the AS (Fig. 6c,f). The vertical distribution of the different groups across the regions revealed that 'nano small' predominated in the Drake region (>50% of total nanophytoplankton abundance), with concentrations up to 4600 cells ml^{-1} (Fig. 6a). South of the PF, this group reappeared homogeneously distributed throughout the water column (Fig. 6d,e). On the other hand, 'nano medium' dominated (on average, 95.8% of total nanophytoplankton abundance) in the waters surrounding the SSI shelf and in the middle of the Bransfield Strait with concentrations over 5000 cells ml^{-1} in the photic layer (Fig. 6b,d). 'Nano large' showed a similar distribution pattern as 'nano medium', but its relative contribution to total nanophytoplankton abundance increased south of the PF (on average, 11.4%). In Fig. 6 we have also included vertical profiles of instantaneous PAR (µmol photons m^{-2} s^{-1}) to show differences between stations sampled in daylight (Fig. 6e) and stations sampled at dawn (Fig. 6b,c), to further discuss phytoplankton photoacclimation.

To introduce the effect of mixing in the irradiance modulation, integrated abundances (cells m^{-2}) (from surface to the MLD) (log-transformed) of the different groups and I_{MLD} (mol photons m^{-2} d^{-1}) were correlated. The 'nano small', 'nano medium' and 'nano large' groups showed a significant negative correlation with I_{MLD} ($r = -0.66$, -0.39 and -0.54, respectively, $p < 0.05$, $N = 26$ to 46). Diel changes, including temporal variability between day and night sampling times in phytoplankton abundances, were explored using surface concentration values. The results did not show significant differences (ANOVA, $p > 0.05$) among sampling times for any of the groups. Finally, averaged cellular diameter values within each phyto-

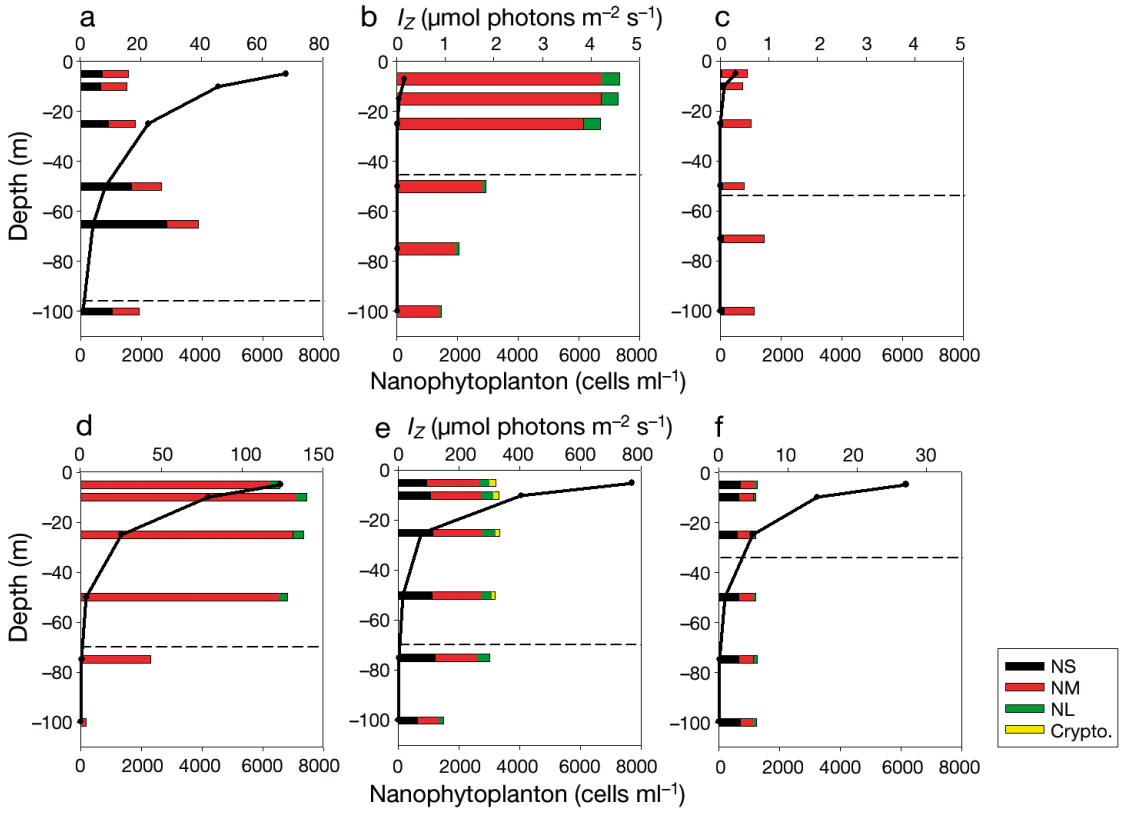

Fig. 6. Vertical profiles of nanophytoplanktonic group abundance and photosynthetically active radiation throughout the water column (I_z, µmol photons m^{-2} s^{-1}) across the different regions: (a) the Drake region; (b) the northern shelf of South Shetland Islands (SSI); (c) between the southern SSI shelf and the Bransfield Front; (d) in the middle of the Bransfield Strait; (e) south of the Peninsula Front; (f) Antarctic Sound (CD1 cast). Dashed line represents the euphotic layer depth. NS: 'nano small'; NM: 'nano medium'; NL: 'nano large'; Crypto.: cryptophytes. Note the different scales for I_z. See García-Muñoz et al. (2013a) for additional figures

plankton group estimated from FCM analysis did not show variations over the studied regions or among sampling times (data not shown).

Photoprotective pigments

Regardless of the sampling depth (surface or DFM), no significant differences (ANOVA, $p > 0.05$) in the photoprotective carotenoids (PPC) to total pigments (TP) ratio (PPC:TP) were detected between stations sampled during the day and at night. However, in those stations where the MLD was deeper than the ZEU, significantly (ANOVA, $p < 0.05$, $N = 7$ stations) higher values were found at the surface. In contrast, at those stations where the ZEU was deeper than the MLD, PPC:TP ratios were more homogeneous between depths and light regimes (data not shown). It was noteworthy that photoprotective pigments were almost absent in the Drake region, whereas the highest ratios were detected around the SSI shelf and the middle of the Bransfield Strait at the surface (Fig. 7). Below this depth, the highest ratios were constrained to the SSI shelf (Fig. 7), significantly correlated ($r = 0.43$, $p < 0.05$, $N = 42$) with the 'nano medium' abundance (cells ml^{-1}) (log-transformed). In the daily cycle of the AS, the highest PPC:TP ratios were detected during the day.

Photosynthetic efficiency variability in the upper water column

Throughout the sampling sites, F_v/F_m only approached the maximum values expected for nutrient-replete conditions (max. $F_v/F_m = 0.65$, e.g. Kolber et al. 1988, Greene et al. 1992) at a few stations at the deepest end of the vertical profile (Fig. 8). Average values of F_v/F_m observed in the upper 100 m varied among stations, not only horizontally, but also vertically (Figs. 8 & 9a). F_v/F_m vertical profiles from all transects showed a dramatic decrease in the upper

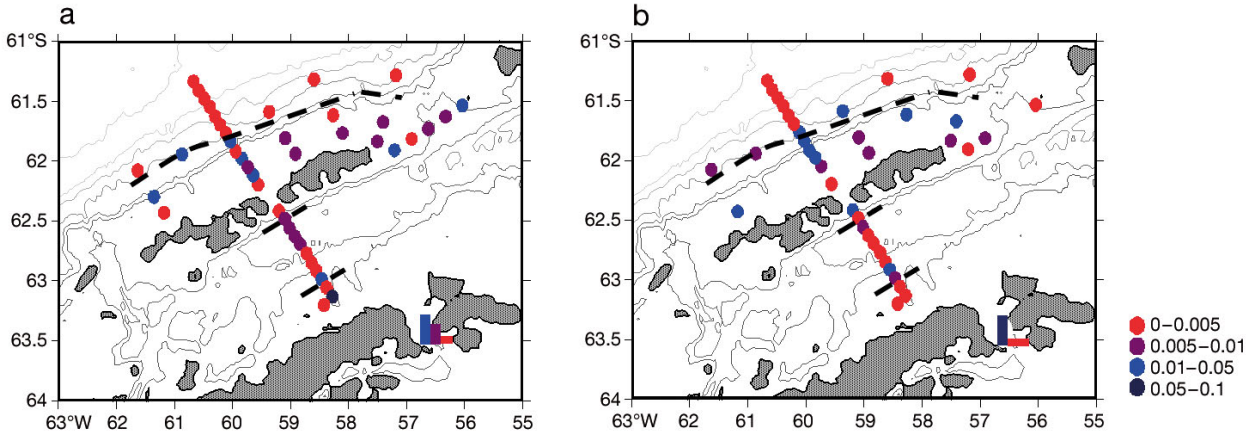

Fig. 7. Photoprotective carotenoids (PPC) to total pigments (TP) ratios throughout the sampling stations at (a) surface and (b) deep fluorescence maximum (below 10 m). Bar graphs at station AS (see Fig. 1) indicate relative results for FRRF casts CD1, CD3 and CD4; dashed lines represent the locations of the fronts, as in Fig. 1

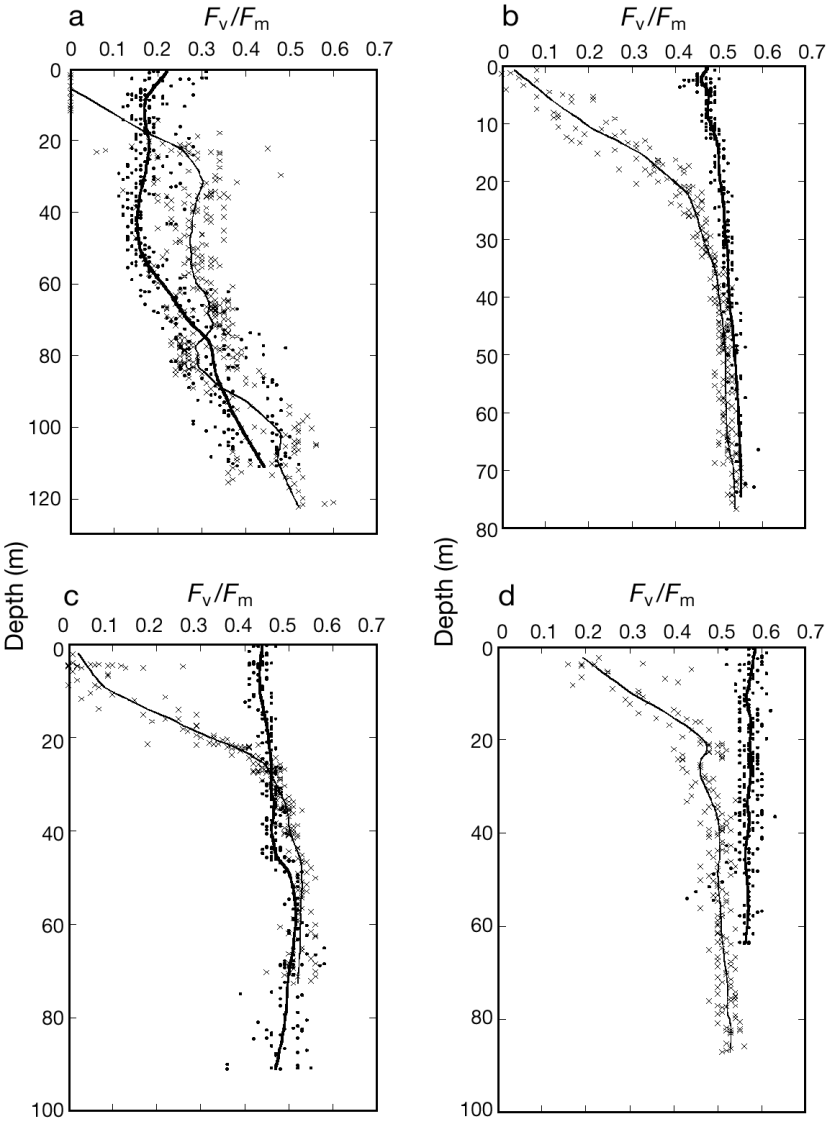

20 m during the day compared with profiles recorded at night (Fig. 8). Values were close to 0 in surface waters at those stations sampled around solar noon, except for the AS region.

In the Drake region, average F_v/F_m in the MLD remained low (<0.4) regardless of sampling time (Figs. 8a & 9a), showing a high vertical variability in each profile (Fig. 8a). The highest F_v/F_m values were detected along the northern SSI shelf (mean ± SD: 0.56 ± 0.03) (Fig. 8b) and in the AS (0.55 ± 0.04) (Fig. 8d). At those stations where the MLD was deeper than the z_{eu}, there was a gradual increase in F_v/F_m with depth within the MLD, while at those stations where the z_{eu} was deeper (mainly north of the archipelago), the main increase was observed below

Fig. 8. Vertical profiles of maximum photosynthetic efficiency (F_v/F_m) values from different stations located in (a) the Drake region; (b) the northern shelf of South Shetland Islands (SSI); (c) in the middle of the Bransfield Strait; and (d) Antarctic Sound (FRRF cast CD2 vs. cast CD4). Each graph shows fast repetition rate fluorometry values recorded during contrasting light conditions: dots correspond to values between 13:00 and 15:00 h and crosses between 05:00 and 06:00 h, except the profile from Bransfield Strait that was recorded at 20:49 h. Curve fit was applied using a 15% smooth to the observed values

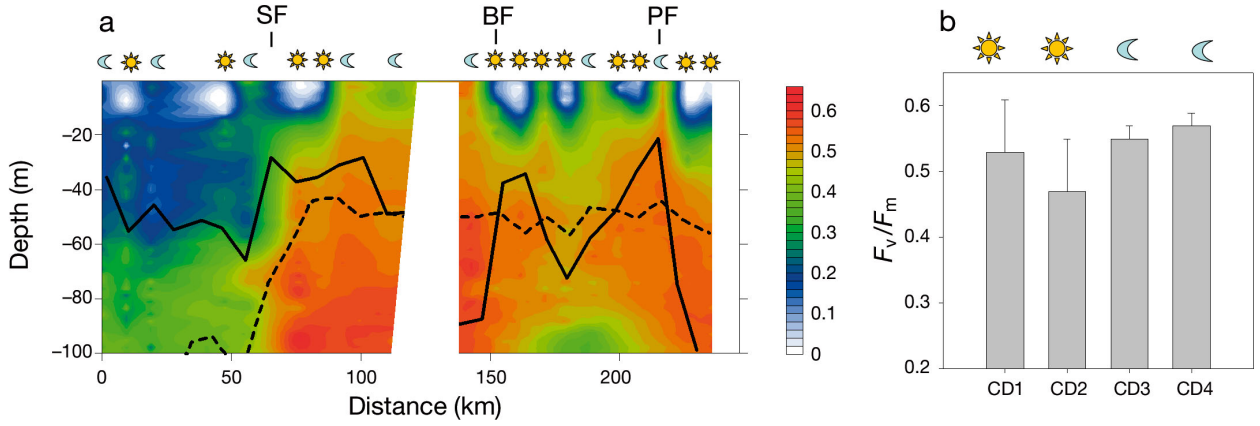

Fig. 9. (a) Maximum photosynthetic efficiency (F_v/F_m) values along transect T.1. The solid line represents the mixed layer depth and the dashed line the euphotic layer depth. BF: Bransfield Front; PF: Peninsula Front; SF: Shetland Front. (b) Mean + SD successive F_v/F_m profiles in the circadian station Antarctic Sound (CD1 to CD4). The sun represents those stations sampled between 06:00 and 18:00 h, and the moon those sampled between 18:00 and 06:00 h

the MLD (Fig. 9). In the daily cycle of the AS, mean F_v/F_m values at the stations with the deepest MLDs (>200 m) remained constant below the first 20 m. Differences between sampling times were tested with 1-way ANOVA, followed by post hoc Tukey's tests. Underwater surface irradiance measured with the FRRF PAR sensor differed significantly ($p < 0.05$) between those stations sampled during the central hours of the day (10:00 to 18:00 h) and dusk and night samples (18:00 to 06:0 h) (Fig. 10). The response of phytoplankton F_v/F_m followed the same significant trend. An almost significant difference ($p = 0.075$) was detected between those stations sampled at dawn (06:00 to 10:00 h) and those sampled during daylight (10:00 to 18:00 h). Surface wind speed, as another environmental variable that could exert variability on F_v/F_m values along a vertical profile, also had a wider range during the day (0.5 to 14.02 m s^{-1}) compared with values recorded at night (3.36 to 9.76 m s^{-1}), but mean values were not significantly different between any of the sampling intervals (Fig. 10).

To avoid diel biasing of surface values due to photoinhibition as shown in Figs. 8 to 10, we eliminated all observations above 20 m, as in Sosik & Olson (2002). Pearson correlations performed between nanophytoplankton groups and F_v/F_m values revealed a significant negative ($r = -0.4$, $p < 0.05$, $N = 136$) relationship between 'nano small' abundance and F_v/F_m values. No positive significant correlations were found with any of the other groups.

The best model obtained using multiple linear regression analysis, explaining the highest variance with the lowest AIC, showed that the main factors controlling photochemical efficiency were the vertical PAR (µmol photon m^{-2} s^{-1}) and the Si* ratio ($N = 136$, deviance: 0.868, $p < 0.001$):

$$F_v/F_m = 0.359 - (0.002 \times \text{vertical PAR}) + (0.004 \times \text{Si}^*) \quad (2)$$

In addition, we also looked for correlations between F_v/F_m and the z_{eu} and MLD. The results showed that there was a significant negative rela-

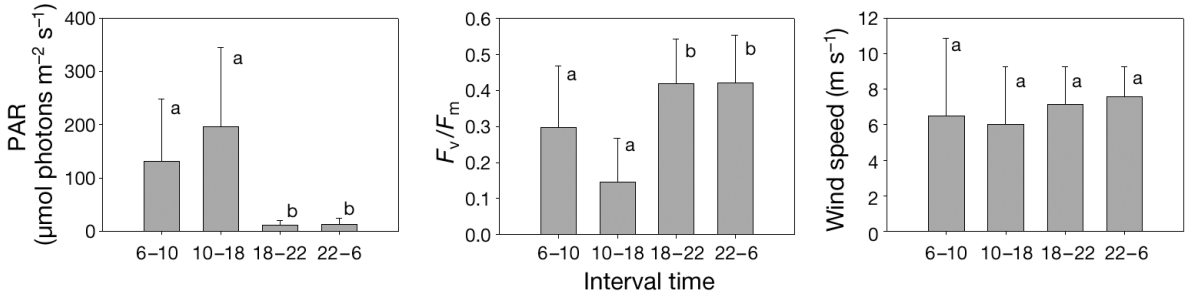

Fig. 10. Mean + SD underwater surface values of photosynthetically active radiation (PAR, µmol photons $m^{-2}s^{-1}$) from the fast repetition rate fluorometry sensor, maximum photosynthetic efficiency (F_v/F_m) and wind speed (m s^{-1}) classified by sampling time (06:00 to 10:00, 10:00 to 18:00, 18:00 to 22:00, 22:00 to 06:00 h). Time intervals sharing letters are not significantly different (Tukey's post hoc honestly significant difference tests, $p < 0.05$).

tionship (r = −0.57, $p < 0.05$) between F_v/F_m and the z_{eu}, mainly due to the deep z_{eu} (>80 m) and low F_v/F_m values found in the Drake region.

DISCUSSION

The descriptive approach utilized by García-Muñoz et al. (2013a) using different analytical methods and the CHEMTAX software revealed that the nanophytoplankton size range dominated around the SSI during the sampling period (>90% of total autotrophic biomass in the Bransfield Strait) and was mainly composed of small diatoms (on average, 79.6% of total nanophytoplanktonic biomass), followed by *Phaeocystis* sp.-like cells (10.7%), prasinophytes (7.2%) and cryptophytes (2.4%). These taxonomic groups were well correlated with the iden- tified FCM groups ('nano medium', 'nano large', 'nano small' and cryptophytes, respectively) (García-Muñoz et al. 2013a). The fractionated chl *a* data presented in this paper ratify the predominance of nanophytoplanktonic cells in almost all regions except AS (Fig. 3f), where microplanktonic diatoms prevailed (García-Muñoz et al. 2013a). Therefore, as diatoms seem to dominate throughout the study area, drawdown nutrient ratios should largely reflect the physiology of the diatoms. In this work, we have shown a detailed description of the spatial (horizontal and vertical) and temporal (on a daily basis) distribution of the physiological state of the phytoplankton assemblage around the SSI. The main results from this study demonstrate that, during the sampling period, there were important differences in the vertical distribution of the phytoplankton groups in relation to irradiance, but physiological indices (F_v/F_m and fluorescence yield) showed spatial patterns across the complex hydrographic regions observed around the SSI. F_v/F_m values ranged from 0.17 in the Drake region to 0.53 in the AS (Fig. 9), whereas the fluorescence yield showed an opposite trend with values higher than 1.1 north of the Shetland Front (Fig. 5), a value that has been used as an indicator for iron-stressed photosynthesis (Holm-Hansen et al. 2000, Hewes et al. 2009). The main variation in F_v/F_m recorded using the dark chamber in samples from ocean waters is known to be a function of cellular health, mainly related to phytoplankton nutrient status as well as to their recent light history (Falkowski & Raven 1994). These results revealed that phytoplanktonic cells were in good physiological conditions in the area surrounding the SSI and towards the Antarctic Peninsula, but started to become stressed at the stations located in the Drake region, where the smaller phytoplankton group (mean ± SD = 2.8 ± 0.2 µm ESD), identified as prasinophytes (García-Muñoz et al. 2013a), predominated. These systematic changes emerged despite substantial mesoscale variability in the region (Sangrà et al. 2011) and in the context of north–south gradients in temperature, salinity (Fig. 2), Si^* ratio (Table 1) and iron (Hewes et al. 2009, Ardelan et al. 2010).

Nutrients

Macronutrient concentrations were always high enough to be non-limiting for phytoplankton growth (Table 1) (Smayda 1997 and references therein) throughout the study area. However, a significant drawdown in the Si^* ratio in the Drake region was evident (Table 1) that was well related to a parallel decrease of total chl *a* (Fig. 3a) and primary production values (Teira et al. 2012, García-Muñoz et al. 2013b), and an increase in fluorescence yield (Fig. 5). High fluorescence yield values have been already reported in the Drake Passage in relation to low iron concentrations (Holm-Hansen et al. 2000). In contrast, low fluorescence yield values towards the Antarctic Peninsula could be related to an increase in iron concentration in this area (Ardelan et al. 2010). Furthermore, Hopkinson et al. (2007) have already linked iron limitation in the Drake region with a low and variable fluorescence ratio, obtained using FRRF, and a significant reduction of the silicic acid: nitrate ratio. Our multiple linear regression analysis strongly supported these previous results, as a positive relationship between F_v/F_m and the Si^* ratio was detected, indicating that phytoplankton cells were less efficient, thus more stressed, under low Si^* ratios. However, south of the Shetland Front, where the F_v/F_m showed healthy growing phytoplankton (Figs. 8 & 9), significant nutrient drawdown had not yet occurred (Table 1), thus indicating that conditions within the Drake region were isolated with respect to chemical and biological processes occurring just outside this region. Iron limitation directly affects phytoplankton photophysiology due to the high iron requirements of the photosynthetic apparatus and electron transport pathways (Arrigo & Alderkamp 2012). These iron requirements in Antarctic phytoplankton vary depending on cell size (Timmermans et al. 2001, Strzepek et al. 2011) and photosynthetic architecture (Strzepek & Harrison 2004, Lavaud et al. 2007), with small cells favoured under iron limitation (Sunda & Huntsman 1997). However, in this study, both nanoplanktonic and microplanktonic chl *a* con-

centrations were significantly correlated with Si*, indicating a possible iron limitation for both smaller and larger phytoplanktonic cells. This fact could be due to the predominance of diatoms both in the nanoplankton and microplankton size range (García-Muñoz et al. 2013a). The ability to assimilate organically complexed iron may differ between phytoplankton taxa (Tagliabue & Arrigo 2005, Strzepek et al. 2011), with diatoms being the most sensitive group, as iron limitation decreases their silicate uptake ability (Hoffmann et al. 2008), which affects frustule formation.

Irradiance

In all the studied areas, photosynthesis was inhibited by midday irradiance at surface waters or by high light at any time during the day (Figs. 8 to 10); moreover, the results showed that there was a significant increase in F_v/F_m surface values at night (Fig. 10). *In situ* inhibition of photosynthesis by near-surface irradiance in Antarctic phytoplankton assemblages has been previously described (Alderkamp et al. 2010, Neale et al. 2012). Our findings also indicated the negative effects of excess irradiance on photosynthetic performance at depths below 20 m, as the multiple linear regression analysis indicated a negative relation between F_v/F_m and vertical PAR. These results agree with the analysis of photoinhibition of polar phytoplankton in East Antarctica performed by Vaillancourt et al. (2003). They showed that photosuppression of F_v/F_m in surface waters was reversible over a time period of minutes to hours. Under high light conditions, the photosynthetic apparatus of phytoplankton is altered, resulting in a reduced functionality that may consist of several effects, from decreased efficiency of energy transfer to reduced capacity for carbon fixation (Neale et al. 2009). In contrast, the highest phytoplankton abundances (mostly 'nano medium', hereafter small diatoms) were detected in surface waters regardless of the sampling time (Fig. 6), and hence is the reason for no positive significant correlations between nanoplanktonic diatom abundance and F_v/F_m values. We have already described how the physical forcing constrained the dominant groups to the surface in the stratified regions associated with the SSI shelf and the fronts (García-Muñoz et al. 2013a), but the underlying processes that promote the predominance of the small diatoms around the SSI archipelago compared with the rest of phytoplankton groups remained unclear. Preliminary results of zooplankton sampled during the cruise showed a spatial segregation of the different taxa, which potentially caused selective grazing (C. García-Muñoz et al. unpubl.). If we focus on the environmental adaptability of phytoplankton groups to determine their proliferation, recent work carried in the study area by Van de Poll et al. (2011) has detected that diatoms show higher photoprotective capacity than haptophytes. Also, Mills et al. (2010) found that diatoms can thrive in shallow mixed layers because their high capacity for heat dissipation minimizes photoinhibition. The ability of diatoms, and to a larger extent other phytoplankton, to occupy a wide range of ecological niches depends critically on their capacity to exploit the differences in the underwater light climate (Lavaud et al. 2007). Interestingly, the highest F_v/F_m values were detected in the SSI shelf and the circadian station (AS) (Figs. 8 & 9), where nanoplanktonic and microplanktonic diatoms dominated, respectively (García-Muñoz et al. 2013a), but contrasting MLDs were detected. Vertical mixing reduces total irradiance, but periodically exposes phytoplankton cells to periods of excessive irradiance when residing near the surface (Alderkamp et al. 2010). If the MLD is deeper than the z_{eu}, phytoplanktonic cells experience changes in light over a relatively short time, from stress-inducing, high light at the surface to undersaturated, low light (or dark) levels, which can lead to short-term changes in cellular pigment content (Kozlowski et al. 2011). Our results indicated that integrated chl *a* <20 µm ESD concentration and nanophytoplankton integrated abundance significantly decayed as the I_{MLD} increased, indicating that this phytoplanktonic size range was highly sensitive to high light levels within the mixed layer. These results provide evidence for a role of photoinhibition in controlling nanophytoplankton distribution around the SSI and towards the Antarctic Peninsula; however in the Drake Passage, the negative relationship between nanophytoplanktonic abundance and I_{MLD} could be indirectly driven by iron limitation. The resulting lower biomass in this region increases the transmission of light in the ocean, decreasing K_d, thus increasing $I_{MLD.}$ On the other hand, the relative contribution of nanoplankton to total chl *a* concentration significantly increased until it reached a maximum, corresponding to mid-irradiances, revealing that smaller cells were better adapted to higher irradiances than larger ones. We can therefore hypothesize that size matters within phytoplanktonic cells in their response to rapid changes in light due to vertical mixing, resulting in a prevalence of nanophytoplankton cells in stratified waters and a predomi-

nance of microplankton under more turbulent conditions (Lavaud et al. 2007). This tight relationship is explored in detail by means of turbulent profiles elsewhere (Sangrà et al. 2014).

Photoacclimation as revealed by pigment ratios

Pigment information can be used to describe the phytoplankton community composition (Mackey et al. 1996), but it can also be used as a proxy for physiological responses to distinct environmental factors (Mendes et al. 2012). In fact, classical Margalef's pigment index reflected this idea as the ratio of an absorbance estimate of the rest of pigments to that of chl *a* (D430/D665) (Margalef 1974), assigning lower values to initial successional stages or less resource-limited media. Today, among the published information, the PPC:TP ratio has been considered remarkably robust for assessing the average physiological state of a phytoplankton community (Barlow et al. 2008, Mendes et al. 2012). It has been previously determined that photoprotective compounds increase during exposure to high PAR and UVR (Van de Poll et al. 2006, Dimier et al. 2007, Villafañe et al. 2008). So information on PPC:TP may thus indicate the previous light history of phytoplankton or, indirectly, other environmental characteristics, such as water column stability (Moline 1998). Significant differences were observed in the PPC:TP ratio in surface waters of those stations where the MLD was deeper than the z_{eu}, supporting the evidence for photoinhibitory stress mentioned above. Our results suggest that photodamage rather than light limitation occurred during the high irradiance portion of the vertical mixing cycle and controlled phytoplankton in those stations with deeper MLDs. In contrast, along the SSI shelf, where shallow MLDs were detected, PPC:TP ratios reached maximum values both at surface and at the DFM (Fig. 7), which was well related to the small diatoms distribution. These results support the hypothesis of a higher photoprotective capacity of small diatoms compared with the rest of the groups and may explain their dominance in stratified coastal waters, as pointed out by Van de Poll et al. (2011).

Further considerations

Surface mixing processes could be driven by strong winds (Mitchell et al. 1991). Wind is also responsible for the amount of time that cells are exposed to high radiation levels (i.e. at or near surface waters). When strong winds conditions occur, algae near the surface can be rapidly transported within a fluctuating light environment from the surface to deeper depths (Villafañe et al. 2008, Neale et al. 2012). During fieldwork of this study, moderate winds prevailed (mean ± SD speed = 6.57 ± 3.08 m s^{-1}), reaching values above 12 m s^{-1} on stormy days, promoting surface vertical mixing processes. Although no general trends were detected between wind speeds and F_v/F_m values, these vertical mixing processes could explain occasional outliers in the F_v/F_m values, e.g. the relative surface maximum found in the middle of Bransfield Strait was at a daytime station (Fig. 9a, F_v/F_m = 0.355, surface mean wind speed = 14 m s^{-1}).

Several studies to date have shown synergies between environmental factors controlling phytoplankton growth, abundance and pigment composition in Antarctic waters (e.g. Timmermans et al. 2001, Hoffmann et al. 2008, Feng et al. 2010, Boyd et al. 2010). Many of them are especially focused towards the effects of light and iron co-limitation. Timmermans et al. (2001) indicated that the growth of small species (including prasinophytes) will hardly ever be halted by low nutrient concentrations (even iron) or low irradiance levels, so the combined iron and light limitation in a specific site of the Southern Ocean will favour the growth of small cells (Sunda & Huntsman 1997). Hoffmann et al. (2008) found that within the diatom taxa, both small and large diatoms were co-limited by silicate and iron, but shallower mixing and the resulting higher irradiance did not favour the growth of the larger species. Furthermore, experiments performed by Strzepek & Harrison (2004) revealed that under high irradiances and iron-replete conditions, cultures of oceanic and coastal diatoms exhibited different behaviour, with coastal cells well adapted to grow under high light exposures. Based on these background studies and the results presented in this study, we can conclude that, across the different mesoscale hydrographic regions explored, several factors interact to control phytoplankton physiological state. In the Drake region, although high I_{MLD} were detected, it appears that cells were less efficient due to an iron limitation rather than photodamage, where deep DFMs were primarily characterised by small prasinophytes, and diatoms were restricted to the south of the Shetland Front. Around the SSI and towards the Antarctic Peninsula, irradiance due to diel differences (day vs. night) and due to water column stability plays a major role in controlling phytoplankton physiological

state. The scenarios of interaction between vertical mixing and phytoplankton photophysiology thus appeared to be different between stations where nanoplankton or microplankton predominated. In this context, small diatoms seemed to be better adapted to highly illuminated, stratified waters, whereas large diatoms were more efficient under lower light regimes, maintaining optimal photosynthetic production in turbulent waters.

Acknowledgements. We are grateful to the captain, crew, and scientists on board RV 'Hespérides' for their co-operation and logistic support during the cruise. Thanks also to E. Ramírez for his assistance in analysing plankton samples, and to B. Mouriño and M. Pérez for providing chlorophyll *a* data. We also thank 3 anonymous reviewers for their valuable comments on a previous version of this manuscript. This work was supported by the CTM2008-06343-C02-02/ANT project from the Spanish Ministry of Science and Education. C.G.M., C.S. and S.M.G.'s work was supported by a predoctoral fellowship from the Spanish Council for Research (CSIC), JAE-Predoc 2009, an Isidro Parga Pondal contract from Xunta de Galicia, and a FPU MEC fellowship, respectively.

LITERATURE CITED

Alderkamp AC, de Baar HJW, Visser RJW, Arrigo KR (2010) Can photoinhibition control phytoplankton abundance in deeply mixed water columns of the Southern Ocean? Limnol Oceanogr 55:1248–1264

Alderkamp AC, Garcon V, de Baar HJW, Arrigo KR (2011) Short-term photoacclimation effects on photoinhibition of phytoplankton in the Drake Passage (Southern Ocean). Deep-Sea Res I 58:943–955

Ardelan MV, Holm-Hansen O, Hewes CD, Reiss CS and others (2010) Natural iron enrichment around the Antarctic Peninsula in the Southern Ocean. Biogeosciences 7: 11–25

Arrigo KR Alderkamp AC (2012) Shedding dynamic light on Fe limitation (DynaLiFe). Deep-Sea Res II 71–76:1–4

Barlow R, Kyewalyanga M, Sessions H, van den Berg M, Morris T (2008) Phytoplankton pigments, functional types, and absorption properties in the Delagoa and Natal Bights of the Agulhas ecosystem. Estuar Coast Shelf Sci 80:201–211

Beardall J, Young E, Roberts S (2001) Approaches for determining phytoplankton nutrient limitation. Aquat Sci 63: 44–69

Behrenfeld MJ, Worthington K, Sherrell RM, Chavez FP, Strutton P, McPhaden MC, Shea DM (2006) Controls on tropical Pacific Ocean productivity. Nature 442: 1025–1028

Boyd PW, Strzepek R, Fu F, Hutchins DA (2010) Environmental control of open-ocean phytoplankton groups: now and in the future. Limnol Oceanogr 55:1353–1376

Coale KH, Johnson KS, Chavez FP, Buesseler KO and others (2004) Southern Ocean iron enrichment experiment: carbon cycling in high- and low-Si waters. Science 304: 408–414

De Jong J, Schoemann V, Lannuzel D, Croot P, de Baar H, Tison JL (2012) Natural iron fertilization of the Atlantic sector of the Southern Ocean by continental shelf sources of the Antarctic Peninsula. J Geophys Res 117: G01029, doi:10.1029/2011JG001679

Dimier C, Corato F, Tramontano F, Brunet C (2007) Photoprotection and xanthophyll cycle activity in three diatoms. J Phycol 43:937–947

Falkowski PG, Raven JA (1994) Aquatic photosynthesis. Blackwell Science, Malden, MA

Feng Y, Hare CE, Rose JM, Handy SM and others (2010) Interactive effects of iron, irradiance and CO_2 on Ross Sea phytoplankton. Deep-Sea Res I 57:368–383

Figueiras FG, Arbones B, Estrada M (1999) Implications of bio-optical modelling of phytoplankton photosynthesis in Antarctic waters: further evidence of no light limitation in the Bransfield Strait. Limnol Oceanogr 44:1599–1608

García MA, Castro CG, Ríos AF, Doval MD, Rosón G, Gomis D, López O (2002) Water masses and distribution of physico-chemical properties in the Western Bransfield Strait and Gerlache Strait during Austral summer 1995/96. Deep-Sea Res II 49:585–602

García-Muñoz C, Lubián LM, García CM, Marrero-Díaz A, Sangrà P, Vernet M (2013a) A mesoscale study of phytoplankton assemblages around the South Shetland Islands (Antarctica). Polar Biol 36:1107–1123

García-Muñoz C, López-Urrutia A, Lubián LM, García CM, Hernández-León S (2013b) A comparison of primary production models in an area of high mesoscale variability (South Shetland Islands, Antarctica). J Sea Res 83:30–39

Geider RJ, La Roche J, Greene RM, Olaizola M (1993) Response of the photosynthetic apparatus of *Phaeodactylum tricornutum* (Bacillariophyceae) to nitrate, phosphate, or iron starvation. J Phycol 29:755–766

Gervais F, Riebesell U, Gorbunov MY (2002) Changes in primary productivity and chlorophyll *a* in response to iron fertilization in the Southern Polar Frontal Zone. Limnol Oceanogr 47:1324–1335

Grasshoff K, Ehrhardt M Kremling K (1983) Methods of seawater analysis. Verlag Chemie, Weinheim

Greene RM, Geider RJ, Kolber Z, Falkowski PG (1992) Iron-induced changes in light harvesting and photochemical energy conversion processes in eukaryotic marine algae. Plant Physiol 100:565–575

Hart TJ (1942) Phytoplankton periodicity in Antarctic surface waters. Disc Rep 21:261–356

Hewes CD, Sakshaug E, Reid FMH, Holm-Hansen O (1990) Microbial autotrophic and heterotrophic eucaryotes in Antarctic waters: relationships between biomass and chlorophyll, adenosine triphosphate and particulate organic carbon. Mar Ecol Prog Ser 63:27–35

Hewes CD, Reiss CS, Kahru M, Mitchell BG, Holm-Hansen O (2008) Control of phytoplankton biomass by dilution and mixed layer depth in the western Weddell-Scotia Confluence. Mar Ecol Prog Ser 366:15–29

Hewes CD, Reiss CS, Holm-Hansen O (2009) A quantitative analysis of sources for summertime phytoplankton variability over 18 years in the South Shetland Islands (Antarctica). Deep-Sea Res I 56:1230–1241

Hoffmann LJ, Peeken I, Lochte K (2008) Iron, silicate, and light co-limitation of three Southern Ocean diatom species. Polar Biol 31:1067–1080

Holm-Hansen O, Amos AF, Hewes CD (2000) Reliability of estimating chlorophyll *a* concentrations in Antarctic waters by measurement of *in situ* chlorophyll *a* fluorescence. Mar Ecol Prog Ser 196:103–110

Hopkinson BM, Mitchell BG, Reynolds RA, Wang H and others (2007) Iron limitation across chlorophyll gradients in the southern Drake Passage: phytoplankton responses to iron addition and photosynthetic indicators of iron stress. Limnol Oceanogr 52:2540–2554

Kang SH, Lee SH (1995) Antarctic phytoplankton assemblage in the western Bransfield Strait region, February 1993: composition, biomass, and mesoscale distributions. Mar Ecol Prog Ser 129:253–267

Kang SH, Kang JS, Lee S, Chung KH, Kim D, Park MG (2001) Antarctic phytoplankton assemblages in the marginal ice zone of the northwestern Weddell Sea. J Plankton Res 23:333–352

Kara AB, Rochford PA, Hurlburt HE (2000) An optimal definition for ocean mixed layer depth. J Geophys Res 105: 16803–16821

Kolber Z, Falkowski PG (1993) Use of active fluorescence to estimate phytoplankton photosynthesis *in situ*. Limnol Oceanogr 38:1646–1665

Kolber Z, Zehr J, Falkowski PG (1988) Effects of growth irradiance and nitrogen limitation on photosynthetic energy conversion in photosystem II. Plant Physiol 88:923–929

Kozlowski W, Deutschman D, Garibotti I, Trees C, Vernet M (2011) An evaluation of the application of CHEMTAX to Antarctic coastal pigment data. Deep-Sea Res I 58: 350–364

Kropuenske LR, Mills MM, van Dijken GL, Bailey S, Robinson DH, Welschmeyer NA, Arrigo KR (2009) Photophysiology in two major Southern Ocean phytoplankton taxa: photoprotection in *Phaeocystis antarctica* and *Fragilariopsis cylindrus*. Limnol Oceanogr 54:1176–1196

Kropuenske LR, Mills MM, van Dijken GL, Alderkamp AC and others (2010) Strategies and rates of photoacclimation in two major Southern Ocean phytoplankton taxa: *Phaeocystis antarctica* (haptophyta) and *Fragilariopsis cylindrus* (bacillariophyceae). J Phycol 46:1138–1151

Lavaud J, Strzepek RF, Kroth PG (2007) Photoprotection capacity differs among diatoms: possible consequences on spatial distribution of diatoms related to fluctuations in the underwater light climate. Limnol Oceanogr 52: 1188–1194

Mackey MD, Mackey DJ, Higgins HW, Wright SW (1996) CHEMTAX — a program for estimating class abundances from chemical markers: application to HPLC measurements of phytoplankton. Mar Ecol Prog Ser 144: 265–283

Margalef R (1974) Ecología. Ediciones Omega, Barcelona

Maxwell K, Johnson GN (2000) Chlorophyll fluorescence — a practical guide. J Exp Bot 51:659–668

Mazzochi MG, Gonzalez HE, Vandromme P, Borrione I and others (2009) A non-diatom plankton bloom controlled by copepod grazing and amphipod predation: preliminary results from the LOHAFEX iron-fertilisation experiment. GLOBEC Int Newsletter 15:3–6

Mendes CRB, de Souza MS, Tavano VM, Costa M, Brotas V, Eiras CA (2012) Dynamics of phytoplankton communities during late summer around the tip of the Antarctic Peninsula. Deep-Sea Res I 65:1–14

Mills MM, Kropuenske LR, van Dijken GL, Alderkamp AC and others (2010) Photophysiology in two Southern Ocean taxa: photosynthesis of *Phaeocystis antarctica* (Prymnesiophyceae) and *Fragilariopsis cylindrus* (Bacillariophyceae) under simulated mixed-layer irradiance. J Phycol 46:1114–1127

Mitchell BG, Brody EA, Holm-Hansen O, McClain C, Bishop J (1991) Light limitation of phytoplankton biomass and macronutrient utilization in the Southern Ocean. Limnol Oceanogr 36:1662–1677

Moline MA (1998) Photoadaptive response during the development of a coastal Antarctic diatom bloom and relationship to water column stability. Limnol Oceanogr 43:146–153

Neale PJ, Jeffrey WH, Sobrino C, Pakulski JD and others (2009) Inhibition of phytoplankton and bacterial productivity by solar radiation in the Ross Sea Polynya. In: Krupnik I, Lang M, Miller S (eds) Smithsonian at the Poles. Contributions to International Polar Year Science. Smithsonian Press, Washington, DC, p 299–308

Neale PJ, Sobrino C, Gargett AE (2012) Vertical mixing and the effects of solar radiation on photosystem II electron transport by phytoplankton in the Ross Sea Polynya. Deep-Sea Res I 63:118–132

Olaizola MJ, La Roche J, Kolber Z, Falkowski PG (1994) Nonphotochemical fluorescence quenching and the diadinoxanthin cycle in a marine diatom. Photosynth Res 41: 357–370

Priddle J, Brandini F, Lipski M, Thorley MR (1994) Pattern of variability of phytoplankton biomass in the Antarctic Peninsula region: an assessment of the BIOMASS cruises. In: El-Sayed SZ (ed) Southern Ocean ecology. Cambridge University Press, Cambridge, p 49–61

Rodríguez F, Varela M, Zapata M (2002) Phytoplankton assemblages in the Gerlache and Bransfield Straits (Antarctic Peninsula) determined by light microscopy and CHEMTAX analysis of HPLC pigment data. Deep-Sea Res II 49:723–747

Sangrà P, Gordo C, Hernádez-Arencibia M, Marrero-Díaz A and others (2011) The Bransfield current system. Deep-Sea Res I 58:390–402

Sangrà P, García-Muñoz C, García CM, Marerro-Diaz A and others (2014) Coupling between the upper ocean layer variability and size-fractionated phytoplankton in a non-nutrient limited environment. Mar Ecol Prog Ser (in press), doi: 10.3354/meps10668

Sarmiento JL, Gruber N, Brzezinski MA, Dunne JP (2004) High-latitude controls of thermocline nutrients and low latitude biological productivity. Nature 427:56–60

Smayda TJ (1997) Harmul algal blooms: their ecophysiology and general relevance to phytoplankton blooms in the sea. Limnol Oceanogr 42:1137–1153

Sosik HM, Olson RJ (2002) Phytoplankton and iron limitation of photosynthetic efficiency in the Southern Ocean during late summer. Deep-Sea Res I 49:1195–1216

Strzepek RF, Harrison PJ (2004) Photosynthetic architecture differs in coastal and oceanic diatoms. Nature 431: 689–692

Strzepek RF, Maldonado MT, Hunter KA, Frew RD, Boyd PW (2011) Adaptive strategies by Southern Ocean phytoplankton to lessen iron limitation: uptake of organically complexed iron and reduced cellular iron requirements. Limnol Oceanogr 56:1983–2002

Sunda WG, Huntsman SA (1997) Interrelated influence of iron, light and cell size on marine phytoplankton growth. Nature 390:389–392

Tagliabue A, Arrigo KR (2005) Iron in the Ross Sea: 1. Impact on CO_2 fluxes via variation in phytoplankton functional group and non-Redfield stoichiometry. J Geophys Res 110:C03009, doi:10.1029/2004JC002531

Teira E, Mouriño-Carballido B, Martínez-García S, Sobrino C, Ameneiro J, Hernández-León S, Vázquez E (2012)

Controls of primary production and bacterial carbon metabolism around South Shetland Islands. Deep-Sea Res I 69:70–81

Timmermans KR, Davey MS, van der Wagt B, Snoek J and others (2001) Co-limitation by iron and light of *Chaetoceros brevis*, *C. dichaeta* and *C. calcitrans* (Bacillariophyceae). Mar Ecol Prog Ser 217:287–297

Ting KC, Giacomelli GA (1987) Availability of solar photosynthetically active radiation. Trans Am Soc Agric Biol Eng 30:1453–1457

UNESCO (1994) Protocols for the Joint Global Ocean Flux Study (JGOFS) core measurements. IOC/SCOR manuals and guides, UNESCO 29:97–100

Vaillancourt RD, Sambrotto RN, Green S, Matsuda A (2003) Phytoplankton biomass and photosynthetic competency in the summertime Mertz Glacier Region of East Antarctica. Deep-Sea Res II 50:1415–1440

Van de Poll WH, van Leeuwe MA, Roggeveld J, Buma AGJ (2005) Nutrient limitation and high irradiance acclimation reduce PAR and UV-induced viability loss in the Antarctic diatom *Chaetoceros brevis* (Bacillariophyceae). J Phycol 41:840–850

Van de Poll WH, Alderkamp AC, Janknegt PJ, Roggeveld J, Buma AGJ (2006) Photoacclimation modulates excessive photosynthetically active and ultraviolet radiation effects in a temperate and Antarctic marine diatom. Limnol Oceanogr 51:1239–1248

Van de Poll WH, Lagunas M, de Vries T, Visser RJW, Buma AGJ (2011) Non-photochemical quenching of chlorophyll fluorescence and xanthophyll cycle responses after excess PAR and UVR in *Chaetoceros brevis*, *Phaeocystis antarctica* and coastal Antarctic phytoplankton. Mar Ecol Prog Ser 426:119–131

Varela M, Fernández E, Serret P (2002) Size-fractionated phytoplankton biomass and primary production in the Gerlache and south Bransfield straits (Antarctic Peninsula) in Austral summer 1995–1996. Deep-Sea Res II 49: 749–768

Vernet M, Kozlowski WA, Yarmey LR, Lowe AT, Ross RM, Quetin LB, Fritsen CH (2012) Primary production throughout austral fall, during a time of decreasing daylength in the western Antarctic Peninsula. Mar Ecol Prog Ser 452:45–61

Villafañe V, Janknegt PJ, de Graaff M, Visser RJW, Van de Poll WH, Buma AGJ, Helbling EW (2008) UVR-induced photoinhibition of summer marine phytoplankton communities from Patagonia. Mar Biol 154:1021–1029

Zapata M, Rodríguez F, Garrido JL (2000) Separation of chlorophylls and carotenoids from marine phytoplankton: a new HPLC method using a reversed phase C_8 column and pyridine-containing mobile phases. Mar Ecol Prog Ser 195:29–45

Editorial responsibility: Steven Lohrenz, New Bedford, Massachusetts, USA

Submitted: March 7, 2013; Accepted: October 14, 2013
Proofs received from author(s): January 27, 2014